



PCCP

**Determinants for proton location and electron coupled
proton transfer in hydrogen bonded pentafluorophenol-
anion clusters**

Journal:	<i>Physical Chemistry Chemical Physics</i>
Manuscript ID	CP-ART-05-2020-002892.R1
Article Type:	Paper
Date Submitted by the Author:	03-Jul-2020
Complete List of Authors:	Zhang, Jian; Donghua University, Chemistry Yang, Yan; East China Normal University, Precision Spectrometry Sun, Zhenrong; East China Normal University, State Key Laboratory of Precision Spectroscopy Wang, Xue-Bin; Pacific Northwest National Laboratory, Physical Sciences Division

SCHOLARONE™
Manuscripts

ARTICLE

Determinants for proton location and electron coupled proton transfer in hydrogen bonded pentafluorophenol-anion clusters

Jian Zhang,^a Yan Yang,^b Zhenrong Sun,^{*b} and Xue-Bin Wang^{*c}

Received 00th January 20xx,
Accepted 00th January 20xx

DOI: 10.1039/x0xx00000x

This work reveals the determinant factors for proton locations and electron coupled proton transfer (ECPT) in biologically relevant hydrogen bonded systems. Pentafluorophenol-anion clusters $[C_6F_5O\cdot H^+\cdot A^-]^-$ are chosen to model active sites of biological functions, with the anion A^- being systematically varied to ensure the proton affinities (PAs) of the anions well cover the referenced PA of $C_6F_5O^-$ from being appreciably smaller, similar, and to significantly larger. Negative ion photoelectron spectroscopy of these clusters provides spectroscopic evidence showing that proton location in the anionic state is largely following the PA prediction, while ECPT is observed only for the clusters with the anion possessing the electron binding energy (EBE) significantly larger than that of the referenced $C_6F_5O^-$. Theoretical calculations suggest these clusters are stabilized by forming single strong hydrogen bond between donor and acceptor, and the associated charge and MO analyses fully support the experimental observations. The current holistic cluster model study indicates that PA is the right determinant that can be used to predict the proton location and describe hydrogen bonding structures, while both PA and EBE of anionic groups play important roles in facilitating ECPT process.

Introduction

Due to the ubiquity of hydrogen bonds in nature, characterizing structures, energetics, and proton transfers of hydrogen bonded systems (HBS) under a variety of contexts has been actively pursued over many decades.¹⁻⁴ The concept of acidity–basicity (pK_a) has been developed to quantify the proton donating–accepting ability of a given substance and to predict the deprotonation–protonation sites in aqueous solutions.⁵ Likewise, gas-phase proton affinity (PA), a thermodynamic quantity measuring the proton acceptance ability of an isolated base, irrelevant to the surrounding environment, provides another perspective for predicting the preferential proton locations of HBS in the gas phase.^{6,7} Studies have shown that the results from aqueous-phase studies may not always transfer to non-aqueous phases, like in ionic liquids and protein active sites of biological systems.^{8,9} And despite considerable experimental evidences showing results in accordance with PA predictions,¹⁰⁻¹² such PA approach has been questioned in several studies of cationic systems¹³⁻¹⁵ and recently also in anionic proton bound clusters.¹⁶⁻²¹ Although considerably broad topics were covered in those studies, the systems in each case were rather very limited. Consequently, the conclusions obtained from these earlier studies are not transportable and appear often

perplexing, suggesting that there exists a considerable knowledge gap in how to describe and predict hydrogen bonding structures and correlate them to well-known macroscopic parameters.

We conceive performing a systematic investigation to probe the structures and energetics of $[X^-\cdot H^+\cdot A^-]$ (A^- , X^- = conjugate bases) proton bound clusters by judiciously choosing different acids, aiming to construct a quantitative model that can predict proton locations based on the known experimental observables. Size-selective negative ion photoelectron spectroscopy (NIPES) is employed to study these proton-bound clusters, because the resulting spectrum encodes important information to characterize the structure of $[X^-\cdot H^+\cdot A^-]$. For example, the spectral pattern of $[X^-\cdot H^+\cdot A^-]$ should bear similarity to that of A^- if HX acts like a solvent spectator. On the other hand, the spectral pattern of the cluster should be very different from either A^- or X^- if the initial structure of $[X^-\cdot H^+\cdot A^-]$ shows a strong proton-sharing property. In addition, NIPES is capable to probe the neutral $[X\cdot H\cdot A]$ structure as well, where the H position in the neutral state is mainly correlated to the bond dissociation energy (BDE) of HA vs. HX. Therefore, NIPES provides an excellent spectroscopic probe to investigate proton or hydrogen atom transfer from $[X^-\cdot HA]$ anion to $[XH\cdot A]$ neutral upon electron detachment,²² a process inherently related to the well-known phenomena of proton-coupled electron transfer reactions that commonly occur in biological systems.²³

^a Key Laboratory of Science and Technology of Eco-Textiles, Ministry of Education, College of Chemistry, Chemical Engineering and Biotechnology, Dong Hua University, Shanghai, 201620, China.

^b State Key Laboratory of Precision Spectroscopy, and Department of Physics, East China Normal University, Shanghai 200062, China. zrsun@phy.ecnu.edu.cn (Z.-R.S).

^c Physical Sciences Division, Pacific Northwest National Laboratory, 902 Battelle Boulevard, P. O. Box 999, MS K8-88, Richland, Washington 99352, USA. xuebin.wang@pnnl.gov (X.-B.W.)

Electronic Supplementary Information (ESI) available: [details of any supplementary information available should be included here]. See DOI: 10.1039/x0xx00000x

ARTICLE

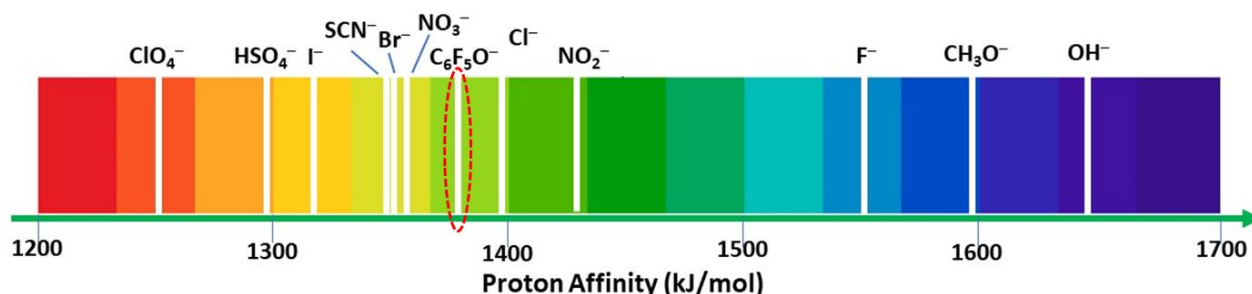


Figure 1. Proton affinities (kJ/mol) of conjugate bases studies in this work.²⁴ The PA of the referenced C₆F₅O⁻ anion is highlighted in red circle.

Herein we present a holistic negative ion photoelectron spectroscopy (NIPES) study over a series of hydrogen bonded clusters with the molecular compositions of [C₆F₅O⁻•H⁺•A⁻], *i.e.*, HX = C₆F₅OH; A = F, Cl, Br, I, SCN, CH₃O, OH, NO₂, NO₃, ClO₄, and HSO₄. We prefer pentafluorophenol over phenol in order to increase the reference HX acidity close to the middle point in the acidity scale across the whole HA series (Figure 1). It is shown that proton locations and binding motif of the anionic complexes are largely determined according to the PA prediction, except for the Cl⁻ case, in which H⁺ bonds to C₆F₅O⁻ albeit its PA being slightly smaller than Cl⁻. Proton transfer upon electron detachment occurs, but only exclusively for the A⁻ = NO₃⁻, HSO₄⁻, and ClO₄⁻ clusters, in which the base anion A⁻ that attracts proton in the neutral state is characterized with possessing appreciably lower PA and much higher electron detachment energy than the corresponding values of C₆F₅O⁻.

Experimental and Theoretical Methodologies

Negative Ion Photoelectron Spectroscopy (NIPES)

The experiments were carried out using a low-temperature NIPES apparatus that consists of an electrospray ionization source, a three-dimensional (3D) cryogenic ion trap, a time-of-flight (TOF) mass spectrometer, and a magnetic-bottle photoelectron analyzer.²⁵ To produce the desired anion complexes [C₆F₅O⁻•H⁺•A⁻]⁻ (A = F–I, SCN, OH, NO₂, NO₃, HSO₄, ClO₄), we used a 10⁻³ molar solution of each related sodium salt mixed with C₆F₅OH in a water/acetonitrile mixture solvent (1/3 volume ratio). For [C₆F₅O⁻•CH₃OH], a 1 mM water/methanol solution of C₆F₅OH was used. The anions produced from electrospray ionization source were guided by two radio frequency quadrupole ion guides and a 90° bender into the 3D cryogenic ion trap, set at 20 K, where they were accumulated and cooled via collisions with a cold buffer gas (~0.1 mTorr, 20% H₂ in helium) for 20–80 ms. The cooling serves to eliminate hot bands and simplify the

spectrum. The cryogenic anions were then pulsed out into the extraction zone of the TOF mass spectrometer for mass-to-charge ratio analyses. In each NIPES experiment, the anions of interest were mass selected and decelerated before interacted with a laser beam in the detachment zone of the magnetic-bottle photoelectron analyzer. Both 193 (6.424 eV) and 157 nm (7.867 eV) photons, generated from ArF and F₂ laser, respectively, were used at a repetition rate of 20 Hz with the ion beam off at alternating laser shots, enabling shot-by-shot background subtraction. Photoelectrons were collected at nearly 100% efficiency by the magnetic bottle and analyzed in a 5.2 m long flight tube. The resultant TOF electron spectrum was converted to kinetic energy spectrum, calibrated with the known spectra of I⁻ and Cu(CN)₂⁻. The electron binding energy spectrum was obtained by subtracting the kinetic energy spectrum from the detachment photon energies used. The energy resolution was about 2%, *i.e.*, 20 meV full width at half maximum for electrons with 1 eV kinetic energy.

Computational Details

Theoretical calculations were carried out to optimize the geometries, to compute the charge distributions, and to perform molecular orbital analyses of the complex anions and corresponding neutrals. All species were optimized using density functional theory (DFT) with the hybrid B3LYP^{26,27} exchange-correlation functional. The 6-311++g(df,pd) basis set²⁸ was used for all atoms except for I, where the LANL2DZ basis set was employed.²⁹ Vibrational frequencies were computed for each optimized structure to ensure that they were energy minima, and the unscaled values were used to obtain the zero-point energies. Single point energy calculations were carried out using the M06-2X^{30–32} method with the basis set of the aug-cc-pvtz for all the elements,³³ and aug-cc-pvtz-pp with the Stuttgart-Köln MCDHF RSC ECP (28 core electrons)³⁴ for I atom, obtained from the EMSL Basis Set Exchange.³⁵ The adiabatic detachment energy (ADE) of the anion was calculated as the energy difference between the corresponding neutral radical and anion each at their respective optimized structures with

zero-point energy corrections. The vertical detachment energy (VDE) was calculated as the energy difference between the neutral and the anion both at the anion's optimized geometry. All calculations were performed with the Gaussian 09 program.³⁶

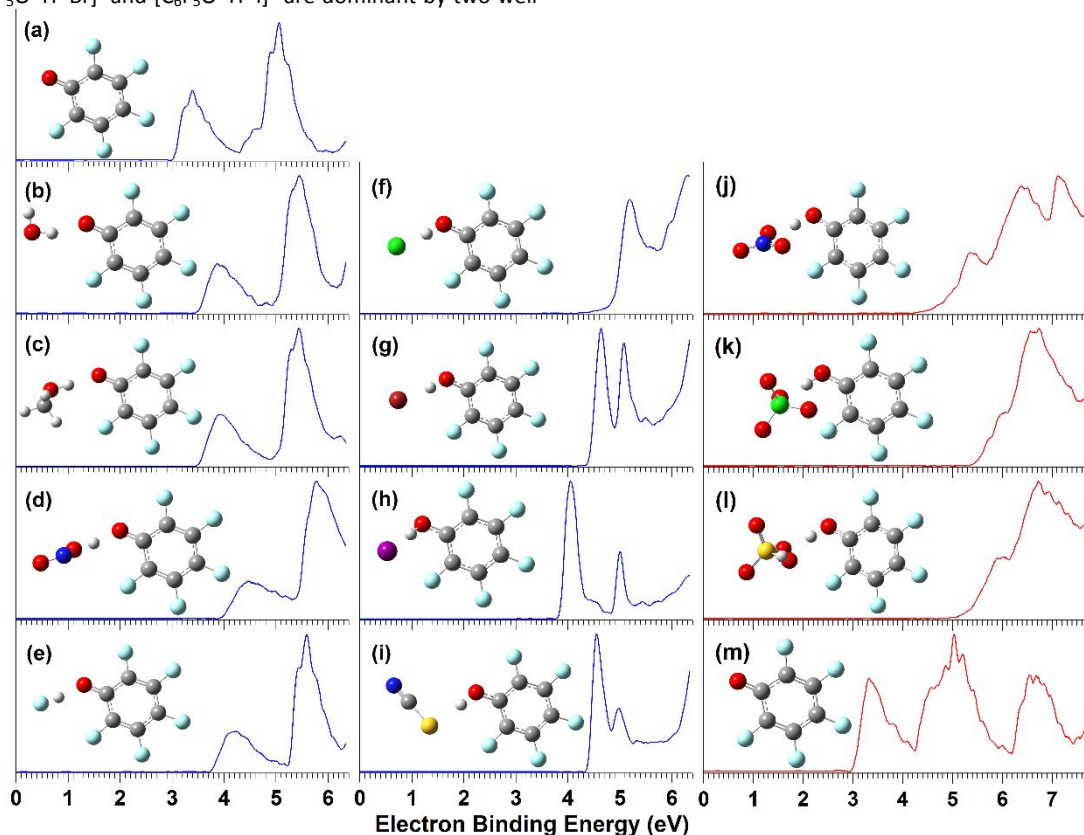
Experimental Results

The low temperature NIPE spectra of $C_6F_5O^-$ (a), $[C_6F_5O \cdot H \cdot A]^-$ A = OH (b), CH_3O (c), NO_2 (d), F (e), Cl (f), Br (g), I (h), SCN (i) at 193 nm (blue); and A = NO_3 (j), ClO_4 (k), HSO_4 (l) at 157 nm, along with the 157 nm spectrum of $C_6F_5O^-$ (m) (red) are shown in Figure 2. Their respective spectra obtained at other wavelengths (266, 157, and 193 nm) are compared in Figure S1. Two broad spectral bands centered at the electron binding energy (EBE) of 3.4 and 5.1 eV are resolved in the 193 nm spectrum of $C_6F_5O^-$. Similar two-band spectral pattern is seen in the 193 nm spectra of $[C_6F_5O \cdot HA]^-$ HA = H_2O (b), CH_3OH (c), HNO_2 (d) and HF (e), but blue-shifts to higher EBE relative to that of $C_6F_5O^-$. This spectral similarity indicates that electrons are photodetached from $C_6F_5O^-$ in these complexes, and HA (= H_2O , CH_3OH , HNO_2 and HF) behaves simply as a solvent molecule. The ADEs / VDEs, determined from the onset threshold / maximum of the first spectral band, are 3.6 / 3.8, 3.6 / 3.9, 4.1 / 4.4, and 3.85 / 4.2 eV, for HA = H_2O , CH_3OH , HNO_2 , and HF complexes, respectively (Table 1).

The spectra of $[C_6F_5O \cdot H \cdot A]^-$, A = Cl, Br, I, and SCN shown in Figure 2(f-i), respectively, are completely different from that of $C_6F_5O^-$. Instead, each spectrum bears similarity to the respective spectrum of A^- , simply blue-shift to high binding energy side. For example, the NIPE spectra of $[C_6F_5O \cdot H \cdot Br]^-$ and $[C_6F_5O \cdot H \cdot I]^-$ are dominant by two well-

resolved peaks, with the energy separations being 0.40, and 0.95 eV for A = Br, and I, respectively, nearly identical to the spin-orbit splitting of Br (0.457 eV) and I atom (0.943 eV).³⁷ Likewise, the first peak in $[C_6F_5O \cdot H \cdot Cl]^-$ and $[C_6F_5O \cdot H \cdot SCN]^-$ spectrum each can be easily identified coming from Cl^- and SCN^- , respectively. Therefore, in these four complexes, the electron emitting chromophores are $A^- = Cl^-$, Br^- , I^- , SCN^- with C_6F_5OH acting like a solvent to stabilize the extra electron on A^- . Careful examination of the $[C_6F_5OH \cdot Cl]^-$ spectrum (Fig. 2f) reveals that besides the main peak with ADE = 4.95 eV, there exists a considerable tail towards low binding energy in spectral threshold region with ADE = 4.5 eV, in contrast to each of those of $[C_6F_5OH \cdot A]^-$ (A = Br, I, SCN) (Fig. 2 g-i), where a sharp onset threshold can be clearly defined. The difference in the appearance of spectral onset regions between the A = Cl case and A = Br / I / SCN cases, although at first glance seems negligible, is in fact quite important, reflecting significantly different bonding nature in $[C_6F_5OH \cdot A]^-$ between A = Cl and A = Br/I/SCN, and will be discussed in the following sections.

Figure 2(j), (k), and (l) are the 157 nm PE spectra of $[C_6F_5O \cdot H \cdot NO_3]^-$, $[C_6F_5O \cdot H \cdot ClO_4]^-$ and $[C_6F_5O \cdot H \cdot HSO_4]^-$, respectively. All three spectra display a long rising onset. The shape of each spectrum is neither like the $C_6F_5O^-$ (Figure 2m) nor the corresponding A^- anion,³⁸⁻⁴⁰ suggesting that the photodetached electrons are neither solely from $C_6F_5O^-$ nor A^- , instead contributed from both them. The ADEs and VDEs of these complexes are all very high, being 4.5, 5.5, 5.3 eV and 5.3, 6.0, 6.0 eV, respectively (Table 1). The comparison of all complex spectra with the shifted $C_6F_5O^-$ and anion A^- spectra is provided in Fig.S2.



ARTICLE

Figure 2. Low-temperature (20 K) photoelectron spectra of $C_6F_5O^-$ (a), $[C_6F_5O \cdot H \cdot A]^-$ A = OH (b), CH_3O (c), NO_2 (d), F (e), Cl (f), Br (g), I (h), SCN (i) at 193 nm (blue); and A = NO_3 (j), ClO_4 (k), HSO_4 (l) at 157 nm, along with the 157 nm spectrum of $C_6F_5O^-$ (m) (red). The B3LYP/6-311++(df,pd) (LANL2DZ for I) optimized anion complex structures are shown as inset. Comparison of the spectra taken at different wavelengths (266, 193, and 157 nm) is provided in Figure S1 in the supporting materials of this manuscript.

Table 1. Experimental and calculated ADEs and VDEs of $[C_6F_5O \cdot H \cdot A]^-$ (in eV).

	Expt. ^a		Calc.	
	ADE	VDE	ADE	VDE
$C_6F_5O^-$	3.1	3.4	3.21	3.45
$[C_6F_5O \cdot H \cdot Br]^-$	4.5	4.7	4.46	4.70
$[C_6F_5O \cdot H \cdot I]^-$	3.95	4.1	3.87	4.06
$[C_6F_5O \cdot H \cdot SCN]^-$	4.5	4.6	4.45	4.68
$[C_6F_5O \cdot H \cdot OCH_3]^-$	3.6	3.9	3.66	3.99
$[C_6F_5O \cdot H \cdot NO_2]^-$	4.1	4.4	4.07 (3.86) ^c	4.54
$[C_6F_5O \cdot H \cdot OH]^-$	3.6	3.8	3.60	3.93
$[C_6F_5O \cdot H \cdot F]^-$	3.85	4.2	3.90	4.28
$[C_6F_5O \cdot H \cdot NO_3]^-$	4.6	5.3	4.34	5.66
$[C_6F_5O \cdot H \cdot ClO_4]^-$	5.5	6.0	4.89	6.24
$[C_6F_5O \cdot H \cdot HSO_4]^-$	5.3	6.0	4.47	6.05
$[C_6F_5O \cdot H \cdot Cl]^-$	4.95, 4.5 ^b	5.2	5.04 (4.20) ^c	5.18

^aExperimental uncertainty is 0.1 eV; ^bADE estimated from the onset of the weak, slowly rising edge; ^cThe numbers in parentheses are calculated ADEs from the optimized neutrals with H being transferred compared to the anionic complexes.

Theoretical Results and discussion

Optimized structures and energetics

Gas-phase structures of anion complexes $[C_6F_5O \cdot H \cdot A]^-$ as well as their corresponding neutrals $[C_6F_5O \cdot H \cdot A]^•$ were optimized, and the anion complex structures are displayed along with their NIPE spectra in Figure 2. Table 2 lists the bond distances of H to O of C_6F_5O , hereby designed as H--O, and H to the anion itself (A) or the nearest O of the anion, hereby called H--A for both the complex anions and neutrals. The bond length of O-H in the isolated C_6F_5OH molecule is calculated to be 0.96 Å, which is in the range of covalent bond. After combining

with the anion of Cl^- , Br^- , I^- and SCN^- , the O-H bond length in $[C_6F_5O \cdot H \cdot A]^-$ modestly increases to 1.06, 1.03, 1.02 and 1.02 Å, respectively. The respective H--A distances in these anion complexes are 1.81, 2.05, 2.33 and 2.04 Å, in the typical H-bond range. These bond length values agree with the experimental results that the H atom is covalently bonded to C_6F_5O and H-bonded to the anions. When the C_6F_5OH molecule interacts with $A^- = CH_3O^-$, NO_2^- , OH^- and F^- anions, the O--H distance dramatically increases to 1.73, 1.46, 1.77 and 1.49 Å, while the H--A bond length decreases to 0.99, 1.05, 0.99 and 0.98 Å, respectively, in formation of $[C_6F_5O \cdot H \cdot A]^-$, HA = CH_3OH , HNO_2 , H_2O , and HF, in which H covalently bound to the anion and interacts with $C_6F_5O^-$ via hydrogen bonding. The predicated structures agree with the

experimental spectra, showing that the detached electrons are from the $C_6F_5O^-$ moiety for each of these four anion complexes. In the complexes $[C_6F_5O \cdot H \cdot NO_3]^-$, $[C_6F_5O \cdot H \cdot ClO_4]^-$ and $[C_6F_5O \cdot H \cdot HSO_4]^-$, the H atom is also covalently bonded to $C_6F_5O^-$ with the O--H bond length slightly increased to 1.05, 1.00 and 1.02 Å, and hydrogen bonded to the anions with the H--A distances of 1.45, 1.61 and 1.52 Å, for A = NO_3 , ClO_4 , and HSO_4 , respectively.

When electrons are photo-detached from the anion clusters, the geometries of the neutral complexes are needed to be re-optimized based on the optimized anion structures. In the neutral complexes $[C_6F_5O \cdot H \cdot A]$, A = Cl, Br, I, SCN, F, OCH_3 , NO_2 , OH, our calculations show

that H atom remains at the same location as in the respective anion complexes, i.e., $[C_6F_5OH \cdot A]$ for the first four, and $[C_6F_5O \cdot HA]$ for the remaining four complexes. However, when the electrons are photo-detached from $[C_6F_5O \cdot H \cdot A]^-$, A = NO_3 , ClO_4 , and HSO_4 , the proton which is initially bound to $C_6F_5O^-$ in the -1 charge state transfers to the anion (A^-) side in the neutral complexes with a typical covalent H--A bond length of ~ 1.0 Å (Table 2). It should be noted that in each of the A = Cl and NO_2 cases, a more stable neutral structure corresponding to the H relocated configuration is identified (by 4.84, 19.37 kcal/mol, for A = NO_2 , Cl, respectively) (see Table 2).

Table 2 The O--H and H--A (anion) bond distances (Å) in the optimized $[C_6F_5O \cdot H \cdot A]^-$ and $[C_6F_5O \cdot H \cdot A]^*$ complexes.

Structural notation		Anion complex		Neutral complex	
		O--H	H--A	O--H	H--A
$[C_6F_5O \cdot H \cdot A]^-$	$[C_6F_5O \cdot H \cdot Br]^-$	1.03	2.05	0.98	2.35
$[C_6F_5O \cdot H \cdot A]^*$	$[C_6F_5O \cdot H \cdot I]^-$	1.02	2.33	0.97	2.89
	$[C_6F_5O \cdot H \cdot SCN]^-$	1.02	2.04	0.97	2.62
$[C_6F_5O \cdot H \cdot A]^-$	$[C_6F_5O \cdot H \cdot OCH_3]^-$	1.73	0.99	2.03	0.96
$[C_6F_5O \cdot H \cdot A]^*$	$[C_6F_5O \cdot H \cdot NO_2]^-$	1.46	1.05	1.87 (0.97) ^a	0.98 (2.07) ^a
	$[C_6F_5O \cdot H \cdot OH]^-$	1.77	0.99	2.02	0.97
	$[C_6F_5O \cdot H \cdot F]^-$	1.49	0.98	1.76	0.94
$[C_6F_5O \cdot H \cdot A]^-$	$[C_6F_5O \cdot H \cdot NO_3]^-$	1.05	1.45	1.76	0.99
$[C_6F_5O \cdot H \cdot A]^*$	$[C_6F_5O \cdot H \cdot ClO_4]^-$	1.00	1.61	1.71	1.00
	$[C_6F_5O \cdot H \cdot HSO_4]^-$	1.02	1.52	1.73	0.99
$[C_6F_5O \cdot H \cdot Cl]^-$	$[C_6F_5O \cdot H \cdot Cl]^-$	1.06	1.81	1.02 (1.96) ^a	1.88 (1.30) ^a
$[C_6F_5O \cdot H \cdot Cl]^*$, $[C_6F_5O \cdot H \cdot Cl]^*$					

^a These bond lengths in parentheses are obtained from the second more stable minimum (by 4.84, 19.37 kcal/mol, for A = NO_2 , Cl, respectively) with H transferred compared to the corresponding initial anionic complexes.

Based on these optimized complex structures in both anionic and neutral states, theoretical ADEs and VDEs are calculated at the M06-2X/aug-cc-pvtz(-pp) // B3LYP/6-311++g(df,pd) (LANL2DZ for I) level of theory and compared with the corresponding experimental values in Table 1. The calculated ADEs and VDEs both are in excellent agreement with the experimental values for the anion clusters $[C_6F_5O \cdot H \cdot A]^-$, A = Br, I, SCN, OCH_3 , NO_2 , OH, and F. However, the calculated ADEs of $[C_6F_5O \cdot H \cdot NO_3]^-$, $[C_6F_5O \cdot H \cdot ClO_4]^-$ and $[C_6F_5O \cdot H \cdot HSO_4]^-$ are significantly smaller than the experimental values. This may attribute to the fact that there is a large structural change from anion to neutral complexes due to the H relocation in these three clusters, resulting in negligible Frank-Condon factors for the transitions from vibrational ground state of the anion to the vibrational ground state of the neutral complexes. In fact, the experimentally determined value represents upper limit of the true ADE for each of the three anion complexes. For

A = Cl, the calculated ADEs from the optimized neutrals without and with H relocation, i.e., $[C_6F_5OH \cdot Cl]$ and $[C_6F_5O \cdot HCl]$ (relative to the anionic state $[C_6F_5OH \cdot Cl]^-$) are 5.04 and 4.20 eV, in good agreement with the experimental values estimated from the main first band and the slowly rising onset in the spectrum (Figure 2f).

The charge distribution, molecular orbital (MO), and bonding analyses

We further carried out the natural bond orbital (NBO) charge distribution analysis for each anion and the respective neutral complexes (Table 3). The molecular frame of each complex can be divided into three parts: C_6F_5O group, H atom and A moiety. As a reference, the C_6F_5O group and H atom carry -0.487 and 0.487 charges respectively in the isolated C_6F_5OH molecule. Four types of charge

distributions can be identified among all complexes studied here based on the NBO charges in $[C_6F_5O \cdot H \cdot A]^-$ and $[C_6F_5O \cdot H \cdot A]^*$. Upon forming complexes with $A^- = Br^-, I^-$ and SCN^- (type I), H atom barely changes its charge (less than 0.01), and most of the extra negative charge remains on the A^- anion (more than -0.83) with the remaining charge being added on C_6F_5O . Upon vertical detachment, the charges on Br^-, I^- and SCN^- anions dramatically decrease by more than 0.7 in magnitude, while the charges on $C_6F_5O^-$ anion are also reduced by 0.3 or 0.2. The change of charges based on natural population analysis (NPA) verifies the experimental results that, in type I anionic complexes, the photodetached electrons are mainly derived from the anions (Br^-, I^- and SCN^-) (>70%), with noticeable contributions from $C_6F_5O^-$. In clusters $[C_6F_5O \cdot H \cdot A]^-$ ($A = OCH_3, NO_2, OH,$ and F) (type II), most of the extra negative charge resides on the C_6F_5O group. The photodetached electrons are overwhelmingly from $C_6F_5O^-$ with less than 10%

contributed from the anions, consistent with the observed spectral patterns. Type III complexes are those with the anions of NO_3^-, ClO_4^- and HSO_4^- hydrogen bonded to C_6F_5OH . The NPA charge analyses indicate that both $C_6F_5O^-$ and the anion contribute to the electron detachment process with comparable ratios (~60/40), a fact that is consistent with the experimental results showing that the spectral pattern is neither like $C_6F_5O^-$ nor the anion. Finally, for $[C_6F_5O \cdot H \cdot Cl]^-$, its NPA charge destitution bears similarity to the type I complexes with only slightly reduced / increased NPA charges for Cl (-0.80) and C_6F_5O (-0.67), relative to the corresponding type I values. However, as indicated by comparing the NPA charge change for $[C_6F_5O \cdot H \cdot Cl]^- \rightarrow [C_6F_5O \cdot H \cdot Cl]^*$, the photodetaching process of this complex removes charges nearly equally from C_6F_5O and Cl moieties, echoing the type III scenario. Therefore $[C_6F_5O \cdot H \cdot Cl]^-$ is singled out as type IV.

Table 3. NPA charge distributions of the $[C_6F_5O \cdot H \cdot A]^-$ complexes and the corresponding unrelaxed neutrals along with electron binding energy (EBE) of the respective free anions (A^-) (in eV)^a

		Anionic / unrelaxed neutral complexes			EBE of free anions A^-
		C_6F_5O	H	A	
	$C_6F_5O \cdot H$	-0.487	0.487		3.1
Type I	$[C_6F_5O \cdot H \cdot Br]^-$	-0.650/-0.307	0.487/0.468	-0.837/-0.161	3.36 ^b
	$[C_6F_5O \cdot H \cdot I]^-$	-0.651/-0.490	0.483/0.461	-0.832/0.029	3.06 ^b
	$[C_6F_5O \cdot H \cdot SCN]^-$	-0.627/-0.439	0.481/0.465	-0.854/-0.026	3.54 ^b
Type II	$[C_6F_5O \cdot H \cdot OCH_3]^-$	-0.958/0.012	0.511/0.481	-0.553/-0.493	1.57 ^b
	$[C_6F_5O \cdot H \cdot NO_2]^-$	-0.881/0.044	0.500/0.482	-0.619/-0.526	2.27 ^b
	$[C_6F_5O \cdot H \cdot OH]^-$	-0.967/0.011	0.507/0.478	-0.540/-0.489	1.83 ^b
	$[C_6F_5O \cdot H \cdot F]^-$	-0.909/0.068	0.559/0.542	-0.650/-0.610	3.40 ^b
Type III	$[C_6F_5O \cdot H \cdot NO_3]^-$	-0.653/-0.090	0.504/0.499	-0.851/-0.409	3.94 ^b
	$[C_6F_5O \cdot H \cdot ClO_4]^-$	-0.599/0.037	0.523/0.526	-0.924/-0.563	5.25 ^b
	$[C_6F_5O \cdot H \cdot HSO_4]^-$	-0.617/-0.06	0.528/0.527	-0.911/-0.467	4.75 ^c
Type IV	$[C_6F_5O \cdot H \cdot Cl]^-$	-0.672/-0.172	0.472/0.456	-0.800/-0.284	3.61 ^b

^a A complete NPA charge distributions of the anion complexes and unrelaxed / optimized neutrals are given in Table S1. ^b Ref. 24. ^c Ref. 40.

The above NPA charge analyses and the suggested electron photo-detached channels are further confirmed and supported by examining the highest occupied MOs (HOMOs) of each anion complex. As shown in Figure 3, the nearly degenerate HOMO and HOMO-1 of complexes $[C_6F_5O \cdot H \cdot A]^-$ for $A^- = Br^-, I^-$ and SCN^- (type I) are dominantly composed of each corresponding anion A^- . For type II complexes with $A^- = OCH_3^-, NO_2^-, OH^-$ and F^- , the HOMO and HOMO-1 reside on the C_6F_5O moiety, while for $[C_6F_5O \cdot H \cdot NO_3]^-$, $[C_6F_5O \cdot H \cdot ClO_4]^-$ and $[C_6F_5O \cdot H \cdot HSO_4]^-$ (type III), HOMO and HOMO-1

delocalize over the entire complex framework including the anions and C_6F_5O parts. According to Koopmans's approximation,⁴¹ the first band with the lowest electron binding energy in each spectrum is derived from detaching one electron from these two iso-degenerate orbitals. The spatial distribution of HOMO and HOMO-1 of these anion complexes and the consequent implication of where the electrons are detached is entirely consistent with the aforementioned NPA charge analyses and also agrees with our experimental results. For $[C_6F_5O \cdot H \cdot Cl]^-$, its HOMO and HOMO-1 consist of Cl and O atomic

orbitals, which, when combined with the NPA charge analysis, suggests that the electron detachment largely only involves Cl and O atoms.

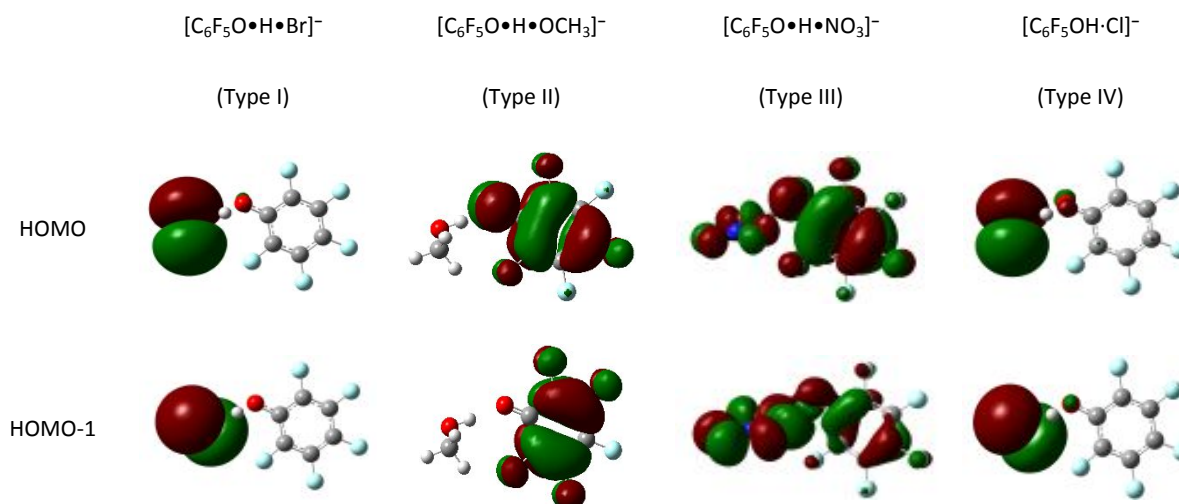


Figure 3. The nearly degenerate HOMO and HOMO-1 for the anion complexes of each type, with $[\text{C}_6\text{F}_5\text{O}\cdot\text{H}\cdot\text{Br}]^-$, $[\text{C}_6\text{F}_5\text{O}\cdot\text{H}\cdot\text{OCH}_3]^-$, $[\text{C}_6\text{F}_5\text{O}\cdot\text{H}\cdot\text{NO}_3]^-$ and $[\text{C}_6\text{F}_5\text{OH}\cdot\text{Cl}]^-$ as a representative for type I, II, III, and IV, respectively (the sets of orbitals of the remaining complexes are provided in Figure S3 in the ESI of this manuscript).

The electron density between the two bonded entities provides a quantitative measure of the degree of covalent bond. Table S2 shows the electron density surfaces of each anion complex plotted using the Multiwfn software.⁴² In complexes $[\text{C}_6\text{F}_5\text{O}\cdot\text{H}\cdot\text{A}]^-$, $\text{A} = \text{Cl}, \text{Br}, \text{I}, \text{SCN}, \text{NO}_3, \text{ClO}_4$ and HSO_4 , the electron densities between $\text{C}_6\text{F}_5\text{O}$ and H atom are large enough to form covalent bond, while the electron densities between H and A are very small. It can be confirmed that the H remains on the $\text{C}_6\text{F}_5\text{O}^-$ side in these complexes. In the $[\text{C}_6\text{F}_5\text{O}\cdot\text{H}\cdot\text{A}]^-$, $\text{A} = \text{CH}_3\text{O}, \text{OH}, \text{NO}_2, \text{F}$ cases, the electron densities between $\text{C}_6\text{F}_5\text{O}$ and H atom are small, but between A and H atom are large, indicating the hydrogen covalently bonded to A with $[\text{C}_6\text{F}_5\text{O}\cdot\text{H}\cdot\text{A}]^-$ structural motif, which is in agreement with the structural optimizations.

Comparison of the proton location in the anionic and neutral complexes

The structures and proton locations in anionic complexes $[\text{C}_6\text{F}_5\text{O}\cdot\text{H}\cdot\text{A}]^-$ are largely determined according to the PA of $\text{C}_6\text{F}_5\text{O}^-$ vs that of A^- . On the one hand, for $\text{A} = \text{Br}, \text{I}, \text{SCN}, \text{NO}_3, \text{ClO}_4$ and HSO_4 , the complexes adopt $[\text{C}_6\text{F}_5\text{OH}\cdot\text{A}]^-$, in which proton is covalently bonded to $\text{C}_6\text{F}_5\text{O}^-$, since PAs of these anions are smaller than the PA of $\text{C}_6\text{F}_5\text{O}^-$ (Figure 1). On the other hand, when $\text{A} = \text{CH}_3\text{O}, \text{OH}, \text{F}, \text{NO}_2$, each anion complex has $[\text{C}_6\text{F}_5\text{O}\cdot\text{H}\cdot\text{A}]^-$ binding motif with H^+ covalently bound to A^- , a fact that also agrees with the PA prediction (PA of A^- larger than PA of $\text{C}_6\text{F}_5\text{O}^-$). One exception is for the Cl case, both experiment and calculation indicate the complex has a structure of $[\text{C}_6\text{F}_5\text{OH}\cdot\text{Cl}]^-$, despite the PA of Cl^- being 23 kJ/mol larger than PA of $\text{C}_6\text{F}_5\text{O}^-$. This 'abnormal' structure may be traced back to the favorable charge (Cl^-)

and dipole ($\text{C}_6\text{F}_5\text{OH}$) interaction embedded in this structure^{43,44} to compensate the PA disadvantage.

The neutral complexes $[\text{C}_6\text{F}_5\text{O}\cdot\text{H}\cdot\text{A}]$, formed upon removal of the excess electron from the corresponding anionic complexes, have in general two minima, $[\text{C}_6\text{F}_5\text{O}\cdot\text{H}\cdot\text{A}]$ and $[\text{C}_6\text{F}_5\text{O}\cdot\text{H}\cdot\text{A}]$. Their relative energies are largely determined by the bond dissociation energy (BDE) differences between $(\text{C}_6\text{F}_5\text{O}\cdot\text{H})$ and $\text{H}\cdot\text{A}$, i.e., the calculated total energy differences of $(\text{C}_6\text{F}_5\text{O}\cdot\text{H} + \text{A}) - (\text{C}_6\text{F}_5\text{O} + \text{H}\cdot\text{A}) \approx \text{BDE}(\text{H}\cdot\text{A}) - \text{BDE}(\text{O}\cdot\text{H})$. Figure 4 shows the PA (left) and BDE difference (right) vs EBE for all anions studied here. It can be concluded that for $\text{A} = \text{CH}_3\text{O}, \text{OH}, \text{F}, \text{Cl}, \text{NO}_3, \text{HSO}_4, \text{ClO}_4$, $[\text{C}_6\text{F}_5\text{O}\cdot\text{H}\cdot\text{A}]$ is energetically more favored; while for $\text{A} = \text{NO}_2, \text{I}, \text{Br}, \text{SCN}$, $[\text{C}_6\text{F}_5\text{O}\cdot\text{H}\cdot\text{A}]$ is more stable. For $\text{A} = \text{I}, \text{Br}, \text{SCN}$, the potential minimum of the anion complex $[\text{C}_6\text{F}_5\text{O}\cdot\text{H}\cdot\text{A}]^-$ lies vertically proximate to the potential well of the neutral $[\text{C}_6\text{F}_5\text{O}\cdot\text{H}\cdot\text{A}]$ (Figure S4), therefore, their NIPE spectra are very similar to the respective spectra of A^- , simply shifts to high binding energy with $\text{C}_6\text{F}_5\text{OH}$ as a spectator solvent. Analogously, the spectra of $[\text{C}_6\text{F}_5\text{O}\cdot\text{H}\cdot\text{A}]^-$, $\text{A} = \text{OH}, \text{CH}_3\text{O}, \text{F}$, appear to match that of $\text{C}_6\text{F}_5\text{O}^-$ with a blue shift in EBE induced by respective HA solvent. The underlying reason is that both anionic and neutral complex, i.e. $[\text{C}_6\text{F}_5\text{O}\cdot\text{H}\cdot\text{A}]^-$ vs $[\text{C}_6\text{F}_5\text{O}\cdot\text{H}\cdot\text{A}]$ adopt similar binding motif with HA behaving like a solvent. However, when the electrons are photo-detached from $[\text{C}_6\text{F}_5\text{OH}\cdot\text{NO}_3]^-$, $[\text{C}_6\text{F}_5\text{OH}\cdot\text{ClO}_4]^-$ and $[\text{C}_6\text{F}_5\text{OH}\cdot\text{HSO}_4]^-$, the proton that is originally on the $\text{C}_6\text{F}_5\text{O}^-$ side in the -1 charge state transfers to the respective anion moiety ($\text{A}^- = \text{NO}_3^-, \text{ClO}_4^-,$ and HSO_4^-) in the neutral state, as evidenced by observing a long slowly rising onset signal in each NIPE spectrum. As shown in Figure S4, for these three complexes,

driven by the significant gain in BDE of H-A over $(\text{C}_6\text{F}_5)\text{O}-\text{H}$ (~ 100 kJ/mol), there is no effective barrier along the proton transfer reaction pathway $[\text{C}_6\text{F}_5\text{O}\cdots\text{H}\cdots\text{A}] \rightarrow [\text{C}_6\text{F}_5\text{O}\cdots\text{H}-\text{A}]$ in the neutral state. Therefore, PT readily occurs upon electron detachment, giving rise to the long rising tail on the threshold region in the spectrum.

For $\text{A} = \text{Cl}$, the anion complex adopts $[\text{C}_6\text{F}_5\text{O}\cdots\text{H}\cdots\text{Cl}]^-$ with O-H and H \cdots Cl bond lengths of 1.06 and 1.81 Å, bearing structural similarity to one of the two minima in the neutral state, i.e. $[\text{C}_6\text{F}_5\text{O}\cdots\text{H}\cdots\text{Cl}]$ with a slightly shortened O-H (1.02 Å) and lengthened H \cdots Cl (1.88 Å) bonds. Vertically detaching the electron from the anion therefore allows access to the geometric topology in the vicinity of $[\text{C}_6\text{F}_5\text{O}\cdots\text{H}\cdots\text{Cl}]$, yielding the main spectral band with the Cl^- spectral characteristic. The other minimum of the neutral with $[\text{C}_6\text{F}_5\text{O}\cdots\text{H}\cdots\text{Cl}]$ structure is 19.37 kcal/mol more stable than $[\text{C}_6\text{F}_5\text{O}\cdots\text{H}\cdots\text{Cl}]$. The Franck-Condon (FC) overlap for $[\text{C}_6\text{F}_5\text{O}\cdots\text{H}\cdots\text{Cl}]^- \rightarrow [\text{C}_6\text{F}_5\text{O}\cdots\text{H}\cdots\text{Cl}]$ is expected to be poor, but apparently not negligible, resulting in a weak long tail toward the low electron binding energy side shown in the spectrum (Figure 2f).

In a similar fashion, there are two minima in the $\text{A} = \text{NO}_2$ case, i.e. $[\text{C}_6\text{F}_5\text{O}\cdots\text{H}\cdots\text{ONO}]^-$ and $[\text{C}_6\text{F}_5\text{O}\cdots\text{H}\cdots\text{ONO}]$ with the latter 4.84 kcal/mol more stable. Detaching $[\text{C}_6\text{F}_5\text{O}\cdots\text{H}\cdots\text{ONO}]^-$ gives rise to spectral features dominant with vertical character, reflecting FC overlaps for $[\text{C}_6\text{F}_5\text{O}\cdots\text{H}\cdots\text{ONO}]^- \rightarrow [\text{C}_6\text{F}_5\text{O}\cdots\text{H}\cdots\text{ONO}]$ (i.e., the spectral band similar to that of $\text{C}_6\text{F}_5\text{O}^-$). However, no obvious long tail towards low binding energy is observed in the threshold of the spectrum, suggesting the FC overlap between $[\text{C}_6\text{F}_5\text{O}\cdots\text{H}\cdots\text{ONO}]^-$ and the more stable, PT transferred, neutral $[\text{C}_6\text{F}_5\text{O}\cdots\text{H}\cdots\text{ONO}]$ is negligible. This might be due to the fact that the barrier separating $[\text{C}_6\text{F}_5\text{O}\cdots\text{H}\cdots\text{ONO}]^-$ and $[\text{C}_6\text{F}_5\text{O}\cdots\text{H}\cdots\text{ONO}]$ being higher because of a less favorable thermodynamic driving force (4.84 kcal/mol for $\text{A} = \text{NO}_2$, vs. 19.37 kcal/mol for $\text{A} = \text{Cl}$).

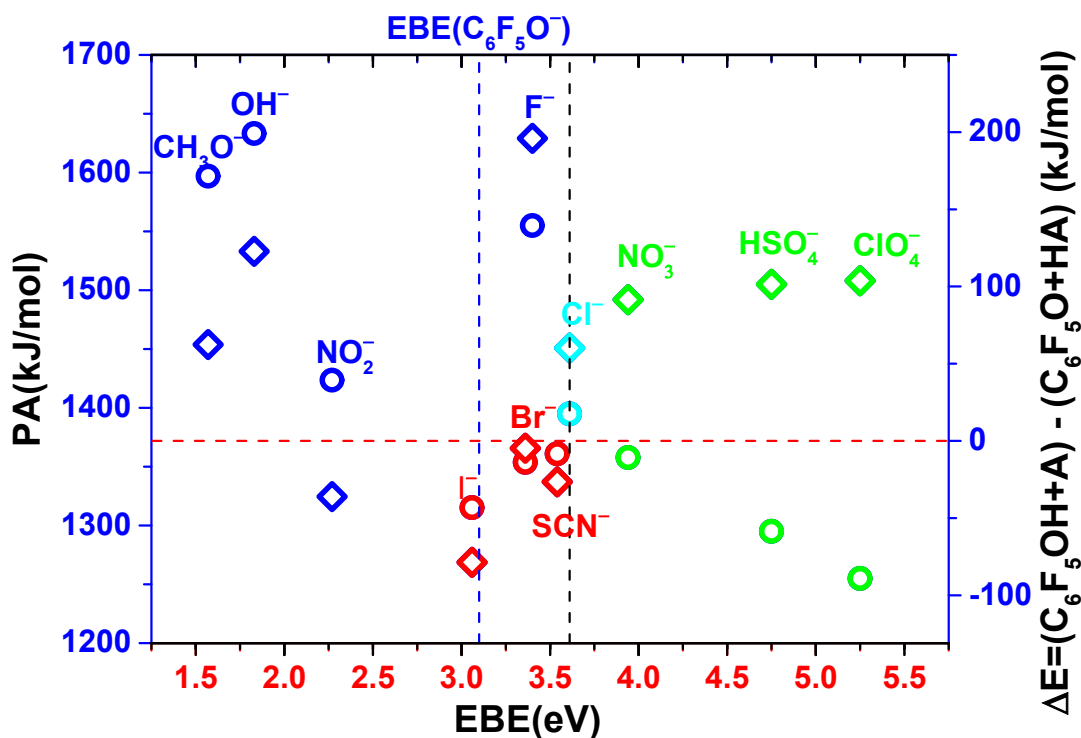


Figure 4. Proton affinity (PA) (circle) and calculated total energy difference of $(\text{C}_6\text{F}_5\text{OH} + \text{A}) - (\text{C}_6\text{F}_5\text{O} + \text{HA}) \approx \text{BDE}(\text{H}-\text{A}) - \text{BDE}(\text{O}-\text{H})$ (diamond) (kJ/mol) vs electron binding energy (EBE) (eV) of all anionic groups studied here. The red dashed horizontal line indicates the PA value of $\text{C}_6\text{F}_5\text{O}^-$, also serves as a reference for $\text{BDE}(\text{H}-\text{A}) = \text{BDE}(\text{O}-\text{H})$. Vertical blue dash line refers the EBE of $\text{C}_6\text{F}_5\text{O}^-$; and vertical black dash line indicates the EBE of Cl^- , from which the complexes with the EBE of A^- larger than that of Cl^- reveal proton transfer in the neutral state upon electron detachment from the initial anionic complexes. Type I, II, III, and IV anions are colour coded as red, blue, green, and turquoise, respectively.

To answer the question why proton transfer occurs upon detaching electrons from complexes $[\text{C}_6\text{F}_5\text{O}\cdots\text{H}\cdots\text{A}]^-$, $\text{A} = \text{NO}_3^-/\text{ClO}_4^-/\text{HSO}_4^-$, but not in the others, we further analyze the HOMOs of each anion complex. The HOMO shows delocalized characteristic and its electron density resides on both $\text{C}_6\text{F}_5\text{O}^-$ and $\text{A}^- = \text{NO}_3^-/\text{ClO}_4^-/\text{HSO}_4^-$ moieties, both contributing to the detached

electrons. Photodetaching these complexes therefore will alter the $\text{C}_6\text{F}_5\text{O}-\text{H}$ and $\text{H}-\text{A}$ bond lengths. As shown above, these three complexes adopt $[\text{C}_6\text{F}_5\text{O}\cdots\text{H}\cdots\text{A}]^-$ in the anionic state, but have $[\text{C}_6\text{F}_5\text{O}\cdots\text{H}-\text{A}]$ structure in the neutral with proton relocated from $\text{C}_6\text{F}_5\text{O}$ to A . Our calculations further indicate there is no or negligible barriers from $[\text{C}_6\text{F}_5\text{O}\cdots\text{H}\cdots\text{A}]^-$ to $[\text{C}_6\text{F}_5\text{O}\cdots\text{H}-\text{A}]$ in the neutral energy surface (Figure S4),

thus facilitating proton transfers. The underlying driving force for such PT transfer is due to the significant larger BDE of H-A than that of C_6F_5O-H . It is interesting to note that in these three complexes where PT occurs with electron removal, the EBE of $C_6F_5O^-$ is significantly smaller than that of A^- ($NO_3^-/ClO_4^-/HSO_4^-$). The fact that the electron on $C_6F_5O^-$ part can be much easily removed than from $NO_3^-/ClO_4^-/HSO_4^-$ part (60% from $C_6F_5O^-$ vs 40% from the respective anion with no charge left on C_6F_5O and ca. -0.5 charge on the anion, Table 3) facilitates PT to form $[C_6F_5O\cdots H-A]$ instead of $[C_6F_5O-H\cdots A]$ as the relocated proton will stabilize the total energy of the neutral complex by combining the positively charged proton with the still negatively charged anion moiety. As comparison, the HOMOs of the rest of anion complexes are all localized, either on A^- side ($Br^-/I^-/SCN^-$) or on $C_6F_5O^-$ part ($A = OCH_3, NO_2, OH, F$). Therefore, photodetachment occurs only on one moiety of the complex with the other part behaving as a spectator. In those cases, the anion and neutral have very similar structures and no PT occurs upon removing electrons. For $[C_6F_5O\cdots H\cdots NO_2]^-$, the anion $[C_6F_5O\cdots H-ONO]^-$ has different structural configuration compared to the lower minimum of the neutral, $[C_6F_5O-H\cdots ONO]$. Because there exists substantial barrier between two minima in the neutral state, and the detachment only occurs on $C_6F_5O^-$ part, no proton relocation upon electron removal is observed. On the contrary, due to the delocalization nature of HOMOs in $[C_6F_5O\cdots H\cdots Cl]^-$ complex, proton transfer process is observed as a minor channel (the weak signal at the threshold on the spectrum) although the major channel is the one without proton transfer.

Conclusions

We have carried out a holistic photoelectron spectroscopic and theoretical investigation on eleven hydrogen-bonded anionic complexes $[C_6F_5O\cdots H\cdots A^-]$ ($A = F, Cl, Br, I, SCN, CH_3O, NO_2, OH, NO_3, ClO_4$ and HSO_4). These complexes are judiciously chosen with the PA of the anion A^- spanning from 1250 to 1650 kJ/mol, well covering the referenced PA of $C_6F_5O^-$ (1372 kJ/mol) with ample examples on both sides of the PA of $C_6F_5O^-$, affording an excellent opportunity to probe acid-base chemistry on these well-defined systems. It is found that anionic complexes $[C_6F_5O\cdots H\cdots A^-]$ adopt $[C_6F_5OH\cdots A^-]$ for $A = Br, I, SCN, NO_3, ClO_4, HSO_4$, while possess binding motif of $[C_6F_5O\cdots HA]$ for $A = CH_3O, NO_2, OH, F$, in which proton is bound to the group with higher PA value, well in line with the acid-base chemistry prediction. The only exception that violates the PA prediction is $[C_6F_5OH\cdots Cl^-]$ (PA of Cl^- being slightly larger than $C_6F_5O^-$), in which proton is bound to $C_6F_5O^-$ driven by favorable charge-dipole interactions. NIPES experiments provide spectroscopic evidence in supporting the above structural identifications with the $A = Br, I, SCN$ spectra showing characteristic A^- signatures, while the $A = CH_3O, NO_2, OH, F$ spectra each displaying $C_6F_5O^-$ pattern. In addition, for the $A = NO_3, ClO_4, HSO_4$ complexes, each NIPE spectrum exhibits a long rising tail in the threshold region, indicating occurrence of proton transfer upon electron detachment, i.e., $[C_6F_5O\cdots H\cdots A^-] \rightarrow [C_6F_5O\cdots H-A]$, driven by stronger H-A BDE. Photodetachment of $[C_6F_5O\cdots H\cdots Cl]^-$ unravels one major channel in forming of $[C_6F_5O-H\cdots Cl]$ and a minor one in formation of $[C_6F_5O\cdots H-Cl]$ with H relocated in the neutral surface. It is interesting to note that for all complexes that proton relocation occurs upon electron removal, the EBEs of the anion A^- ($Cl^-, NO_3^-, ClO_4^-, HSO_4^-$) are all significantly larger than the EBE of $C_6F_5O^-$. This phenomenological observation illustrates

that there is the electronic origin for the PT in the neutral state, that is, because the detached electron is largely derived from the $C_6F_5O^-$ group, the formed neutral complexes are stabilized by transferring the proton to neutralize the A^- part. The detailed information on the structures, energetics, and electron-detachment-induced proton transfer over this series of hydrogen-bonded complexes illustrates rich acid-base chemistry at cluster scale and may help better understand relevant chemistry and PT process in active sites of biological systems.

Conflicts of interest

There are no conflicts to declare.

Acknowledgements

This work was supported by U.S. Department of Energy (DOE), Office of Basic Energy Sciences, Division of Chemical Sciences, Geosciences, and Biosciences (X.-B.W.), and performed using EMSL, a national scientific user facility sponsored by DOE's Office of Biological and Environmental Research and located at Pacific Northwest National Laboratory, which is operated by Battelle Memorial Institute for the DOE. Part of this work was supported by the National Natural Science Foundation of China (No-11604046 for JZ; No. 11727810 for ZRS), as well as "Chenguang Program" by Shanghai Education Development Foundation, Shanghai Municipal Education Commission (No. 16CG38) and Natural Science Foundation of Shanghai (No. 16ZR1448100) (JZ).

Notes and references

- 1 R. S. Blake, P. S. Monks, A. M. Ellis, *Chem. Rev.* **2009**, **109**, 861-896.
- 2 S. J. Ferguson, *Curr. Biol.* **2000**, **10**, R627-R630.
- 3 R. P. Bell, *The Proton in Chemistry*, Second Edition, Springer US, Fletcher & Son Ltd, Norwich, 1973.
- 4 C. T. Wolke, J. A. Fournier, L. C. Dzugan, M. R. Fagiani, T. T. Odbadrakh, H. Knorke, K. D. Jordan, A. B. McCoy, K. R. Asmis, M. A. Johnson, *Science*, **2016**, **354**, 1131-1135.
- 5 J. N. Brønsted, *Rec. des Trav. Chim. Pays-Bas* **1923**, **42**, 718-728.
- 6 R. G. Cooks, P. S. H. Wong, *Acc. Chem. Res.* **1998**, **31**, 379-386.
- 7 R. G. Cooks, J. T. Koskinen, P. D. Thomas, *J. Mass Spectrom.* **1999**, **34**, 85-92.
- 8 K. E. Johnson, R. M. Pagni, J. Bartmess, *J. Monatsh. Chem.* **2007**, **138**, 1077-1101.
- 9 B. Elsasser, M. Valiev, J. H. Weare, *J. Am. Chem. Soc.* **2009**, **131**, 3869-3871.
- 10 S. Sato, N. Mikami, *J. Phys. Chem.* **1996**, **100**, 4765-4769.
- 11 J. R. Roscioli, L. R. McCunn, M. A. Johnson, *Science*, **2007**, **316**, 249-254.
- 12 G. E. Douberly, A. M. Ricks, B. W. Ticknor, M. A. Duncan, *Phys. Chem. Chem. Phys.* **2008**, **10**, 77-79.
- 13 T. D. Fridgen, *J. Phys. Chem. A* **2006**, **110**, 6122.
- 14 T. C. Cheng, B. Bandyopadhyay, J. D. Mosley, M. A. Duncan, *J. Am. Chem. Soc.* **2012**, **134**, 13046-13055.
- 15 D. Bing, T. Hamashima, C.-W. Tsai, A. Fujii, J.-L. Kuo, *Chem. Phys.* **2013**, **421**, 1-9.
- 16 T. I. Yacovitch, N. Heine, C. Brieger, T. Wende, C. Hock, D. M. Neumark, K. R. Asmis, *J. Chem. Phys.* **2012**, **136**, 241102.
- 17 G.-L. Hou, W. Lin, S. H. M. Deng, J. Zhang, W.-J. Zheng, F. Paesani, X.-B. Wang, *J. Phys. Chem. Lett.* **2013**, **4**, 779-785.
- 18 E. V. Beletskiy, X.-B. Wang, S. R. Kass, *J. Phys. Chem. A* **2016**, **120**, 8309-8316.

- 19 G.-L. Hou, X.-B. Wang, M. Valiev, *J. Am. Chem. Soc.* 2017, **139**, 11321-11324.
- 20 G.-L. Hou, W. Lin, X.-B. Wang, *Communications Chemistry* 2018, **1**, 37.
- 21 G.-L. Hou, M. Valiev, X.-B. Wang, *Int. J. Mass Spectrom.* 2019, **439**, 27-33.
- 22 X.-B. Wang, S. R. Kass, *J. Am. Chem. Soc.* 2014, **136**, 17332-17336.
- 23 A. K. Harshan, T. Yu, A. V. Soudackov, Sharon Hammes-Schiffer, *J. Am. Chem. Soc.* 2015, **137**, 13545-13555.
- 24 E. P. J. Linstrom, W. J. Mallard, *NIST Chemistry WebBook, Nist Standard Reference Database Number 69*; National Institute of Standards and Technology: Gaithersburg MD, 20899. <https://doi.org/10.18434/T4D303> (retrieved March 15, 2020).
- 25 X.-B. Wang and L.-S. Wang, *Rev. Sci. Instrum.*, 2008, **79**, 073108.
- 26 A. D. Becke, *J. Chem. Phys.* 1993, **98**, 5648–5652.
- 27 C. Lee, W. Yang, R. G. Parr, *Phys. Rev. B* 1988, **37 (2)**, 785–789.
- 28 R. Krishnan, J. S. Binkley, R. Seeger, J. A. Pople, *J. Chem. Phys.* 1980, **72**, 650–654.
- 29 P. J. Hay and W. R. Wadt, *J. Chem. Phys.* 1985, **82**, 270-283.
- 30 Y. Zhao and D. G. Truhlar, *J. Phys. Chem. A*, 2008, **112**, 1095-1099.
- 31 Y. Zhao and D. G. Truhlar, *Theor. Chem. Acc.*, 2008, **120**, 215-241.
- 32 Y. Zhao and D. G. Truhlar, *Acc. Chem. Res.*, 2008, **41**, 157-167.
- 33 T. H. Dunning Jr. *J. Chem. Phys.* 1989, **90**, 1007.
- 34 K. A. Peterson, B. C. Shepler, D. Figgen, H. Stoll, *J. Phys. Chem. A* 2006, **110**, 13877.
- 35 K. L. Schuchardt, B. T. Didier, T. Elsethagen, L. Sun, V. Gurumoorthi, J. Chase, J. Li, T. L. Windus, *J. Chem. Inf. Model.* 2007, **47**, 1045-1052.
- 36 M. J. Frisch, G. W. Trucks, H. B. Schlegel, G. E. Scuseria, M. A. Robb, J. R. Cheeseman, G. Scalmani, V. Barone, B. Mennucci and G. A. Petersson, et al., Gaussian 09, Gaussian, Inc., Wallingford CT, 2009.
- 37 D. W. Arnold, S. E. Bradforth, E. H. Kim and D. M. Neumark, *J. Chem. Phys.*, 1995, **102**, 3493.
- 38 X. B. Wang, X. Yang, L. S. Wang, and J. B. Nicholas, *J. B. J. Chem. Phys.*, 2002, **116**, 561-570.
- 39 X. B. Wang and L. S. Wang, *J. Chem. Phys.* 2000, **113**, 10928-10933.
- 40 G. L. Hou, W. Lin, S. H. M. Deng, J. Zhang, W. Zheng, F. Paesani, X.-B. Wang, *J. Phys. Chem. Lett.* 2013, **4**, 779-785.
- 41 D. J. Tozer and N. C. Handy, *J. Chem. Phys.* 1998, **109**, 10180-10189.
- 42 T. Lu and F. Chen, *J. Comput. Chem.* 2012, **33**, 580-592.
- 43 T.D. Fridgen, *J. Phys. Chem. A* 2006, **110**, 6122-6128.
- 44 L. Wang, Q. Yuan, W. Cao, J. Han, X. Zhou, S. Liu, and X.-B. Wang, *J. Phys. Chem. A* 2020, **124**, 2036-2045.